
Manifold-Matching Autoencoders

Laurent Cheret¹ Vincent Létourneau² Isar Nejadgholi³ Chris Drummond³ Hussein Al Osman¹
Maia Fraser¹

Abstract

We study a simple unsupervised regularization scheme for autoencoders called Manifold-Matching (MMAE): we align the pairwise distances in the latent space to those of the input data space by minimizing mean squared error. Because alignment occurs on pairwise distances rather than coordinates, it can also be extended to a lower dimensional representation of the data, adding flexibility to the method. We found that this regularization outperforms similar methods on metrics based on preservation of closest neighbors distances and persistence homology based measures. We also observe MMAE provides a scalable approximation of ‘Multi-Dimensional Scaling’ (MDS).

1. Introduction

Dimensionality reduction is fundamental to modern data analysis, enabling visualization and interpretation of high-dimensional datasets. Autoencoders (Hinton & Salakhutdinov, 2006; Chen & Guo, 2023) learn compressed representations by minimizing reconstruction error, but this objective alone does not guarantee preservation of any particular geometric or topological structure. When the encoder ignores these structures, similar objects in the input space may be mapped to distinct regions of the latent space, creating discontinuities that negatively affect the decoder’s ability to reconstruct (Batson et al., 2021). This problem can also affect other downstream tasks. For example, in anomaly detection or when visualizing developmental trajectories in single-cell data (Chari & Pachter, 2023) or exploring latent spaces in generative models (Chadebec & Allasonnière, 2022; Xu et al., 2024)—additional regularization becomes necessary.

¹Department of Computer Science, University of Ottawa, Ottawa, Canada ²MILA, Montréal, Canada ³National Research Council of Canada, Ottawa, Canada. Correspondence to: Laurent Cheret <lcher021@uottawa.ca>.

1.1. Topology and Geometry in Autoencoders

Following the success of statistical methods using topological data analysis tools like persistence diagrams (Su et al.), there has been a recent effort to improve the preservation of topological features by autoencoders, which we classify as topological or geometrical methods. **Topological methods** (Moor et al., 2020b; Trofimov et al., 2023) use persistent homology to identify and preserve multi-scale structural features such as connected components, loops, and voids. **Geometric methods** (Singh & Nag, 2021; Nazari et al., 2023; Lim et al., 2024) focus on preserving local angles and distances.

Take, for example, the nested spheres dataset (Moor et al., 2020b), a simple synthetic yet highly nonlinear case: ten 100-dimensional small spheres are nested inside a larger 100D enclosing sphere. A topologically accurate 2D representation should preserve this nesting relationship, with the outer sphere cluster surrounding the inner sphere clusters. To date, only topological autoencoder variants consistently recover this structure in 2D/3D. Other autoencoder variants and nonparametric methods such as UMAP (McInnes et al., 2018), t-SNE (van der Maaten & Hinton, 2008), and PHATE (Moon et al., 2017) fail in this case. Interestingly, we found that the classical method Multidimensional Scaling (MDS) (Torgerson, 1952) also successfully recovers the nesting relationship—a result that, to the best of our knowledge, has not been reported in previous work.

1.2. Our Approach: Alignment of Pairwise Distances

Classical MDS (Torgerson, 1952) utilizes the pairwise distance matrix of the entire dataset to preserve global geometry. In contrast, topological autoencoders like TopoAE (Moor et al., 2020b) and RTD-AE (Trofimov et al., 2023) employ persistent homology signatures on pairwise distance matrices at the mini-batch level. While the former focuses on geometric distances—which may implicitly capture topology—the latter prioritize multi-scale structural connectivity, a focus that has been shown to result in superior preservation of the manifold’s global geometry. One issue arises with these methods, MDS scales poorly with data size due to memory requirements to compute the $n \times n$ pairwise distance matrix, and topological variants of au-

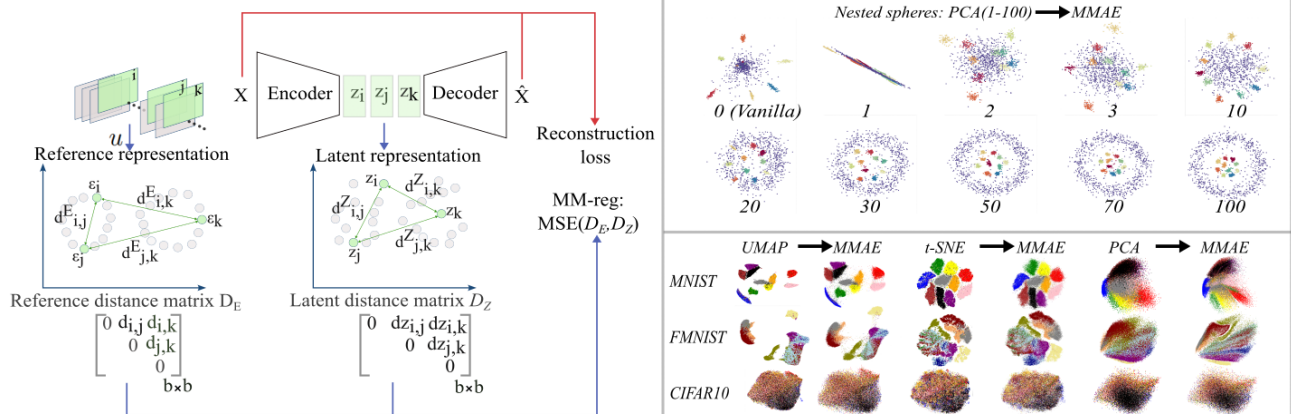


Figure 1. **Left:** Overview of the current approach. The Manifold-Matching regularization $MM\text{-reg}$ is added to the objective function of the standard AE, forming MMAEs. **Top Right:** 2D latent spaces of the Nested Spheres dataset (Moor et al., 2020b). Standard AE (Vanilla) using no MM-reg and 9 MMAE models using different number of PCA components in their regularization (1 \rightarrow 100). **Bottom Right:** MMAE 2D latent spaces “copying” 2D embeddings from UMAP, t-SNE, and PCA across MNIST, F-MNIST, and CIFAR10 datasets.

toencoders scale poorly with the batch size b due to the persistent homology computations batch-wise. A central question emerges: *What happens to latent spaces when global geometry preservation is imposed in autoencoders?*

We address this by introducing a regularization term called Manifold-Matching (MM-reg), defined as the MSE between the pairwise distance matrix D_Z of the latent space and a reference distance matrix D_E computed from either the input data X itself or its respective embedding. Crucially, since both D_Z and D_E are $b \times b$ matrices (where b is the batch size), the dimensionality of the reference space is decoupled from the bottleneck dimensionality. This means, for example, that a 2D latent space can be regularized using distances from a 50D or 100D reference representation.

Note there is strong theoretical justification in the choice to replace the data by its distance matrix. In short, distance preservation implies topology preservation. This is the content of section 2.2.

Figure 1 illustrates this effect on the nested spheres dataset. Without regularization, the standard AE projects the inner spheres outside the cluster representing the outer sphere, consistent with prior literature. However, with MM-reg, as the number of PCA components in the reference increases, the nesting structure present in the original data emerges, with the inner sphere clusters progressively pulled inside the outer sphere cluster. In the specific case in which the reference embeddings are 2D, a “copying” effect can be seen where the 2D latent space approximates the reference, allowing the autoencoder to extend known representation to new data points.

Specifically, our **contributions** are: **(1)** We introduce the **Manifold-Matching Autoencoder (MMAE)**, an unsuper-

vised framework for global structure-aware dimensionality reduction. **(2)** We study its visualization effects on synthetic datasets where the topology is intuitively understood. **(3)** We extend experiments to real-world benchmarks, showing competitive performance against topological and geometrical autoencoder variants. **(4)** We provide discussions on global geometry preservation as a proxy for topology preservation.

2. Background

We review the key concepts underlying our approach: persistent homology as the gold standard for topological comparison, and the relation between distance preservation and topology.

2.1. Persistent Homology

The importance of understanding data topology has been recognized since the 1960s (Rosenblatt, 1962). This concern is tied to the manifold hypothesis: high-dimensional data $\mathbf{X} = \{\mathbf{x}_i\}_{i=1}^k$ with $\mathbf{x}_i \in \mathbb{R}^n$ typically lies on or near a lower-dimensional manifold $\mathcal{M} \subset \mathbb{R}^n$. Persistent homology provides a principled way to detect the topological features of this manifold across scales (Edelsbrunner et al., 2002; Carlsson, 2009).

2.2. From Distance Preservation to Topology Preservation

Multidimensional Scaling (MDS) (Torgerson, 1952) provides a classical approach that finds a low-dimensional configuration of points whose pairwise distances best preserve those of the input distance matrix. The key insight is that

while points $\mathbf{x}_i, \mathbf{x}_j \in \mathbb{R}^n$ may have many coordinates, their Euclidean distance $d_{ij} = \|\mathbf{x}_i - \mathbf{x}_j\|_2$ reduces their relationship to a single scalar value. Remarkably, collecting all such pairwise distances into a matrix \mathbf{D} contains sufficient information to recover the original geometric configuration. Classical MDS formalizes this by converting distance relationships into geometric configurations through eigendecomposition of the associated Gram matrix (Borg & Groenen, 2005; Schoenberg, 1935).

This distance-centric view connects naturally to topology preservation through the stability theorem. For finite metric spaces with Vietoris-Rips persistence diagrams:

Theorem 2.1 (Stability (Cohen-Steiner et al., 2007; Chazal et al., 2016)).

$$d_B(\text{Dgm}_p(X), \text{Dgm}_p(Y)) \leq 2 \cdot d_{GH}(X, Y) \quad (1)$$

for all homology dimensions $p \geq 0$, where d_B is the bottleneck distance and d_{GH} the Gromov-Hausdorff distance.

Since uniform distance preservation bounds d_{GH} , we obtain:

Corollary 2.2 (Distance Preservation Implies Topology Preservation). *If an encoder f_θ satisfies $|d_X(x_i, x_j) - d_Z(f_\theta(x_i), f_\theta(x_j))| \leq \epsilon$ for all pairs, then $d_B(\text{Dgm}_p(X), \text{Dgm}_p(f_\theta(X))) \leq 2\epsilon$ for all $p \geq 0$.*

This result reveals our path forward: rather than computing persistent homology during training, we preserve topology by preserving distances. Manifold-Matching Autoencoders operationalize this principle by aligning the latent space to a reference geometry through pairwise distances. In practice, MMAE applies this principle at the minibatch level, leveraging the theoretical justification that batch-wise topology approximates global topology as batch size increases.

A practical consideration is that training operates on minibatches rather than the full dataset. TopoAE (Moor et al., 2020b) provides theoretical justification for this approach through two key results. First, they establish that the probability of batch topology deviating from full set topology is bounded by geometric sampling:

$$\begin{aligned} P(d_B(\text{Dgm}(X), \text{Dgm}(X^{(b)})) > \epsilon) \\ \leq P(d_H(X, X^{(b)}) > \frac{\epsilon}{2}) \end{aligned} \quad (2)$$

where $X^{(b)}$ is a mini-batch of size b and d_H is the Hausdorff distance. Second, they show that as batch size approaches dataset size, the expected Hausdorff distance converges to zero, meaning batch-level topology increasingly mirrors global topology. This justifies using batch-wise distance preservation as a proxy for global structure preservation.

3. Related Work

The challenge of learning topologically correct representations has motivated several autoencoder variants. We review these methods through our core question: how can we capture global structure efficiently?

3.1. Topological Autoencoders

TopoAE (Moor et al., 2020b) pioneered using persistent homology as a training signal. Given distance matrices D_X and D_Z in input and latent space, it penalizes discrepancies between topologically significant point pairs:

$$\mathcal{L}_{\text{topo}} = \frac{1}{2} \sum_{(i,j) \in \mathcal{P}_X} (D_X^{ij} - D_Z^{ij})^2 + \frac{1}{2} \sum_{(k,l) \in \mathcal{P}_Z} (D_Z^{kl} - D_X^{kl})^2 \quad (3)$$

where $\mathcal{P}_X, \mathcal{P}_Z$ denote topologically significant pairs (births/deaths in persistence diagrams). While theoretically generalizable, the implementation focuses on H_0 (connected components) via minimum spanning trees for efficiency. Two limitations arise: (1) the loss is discontinuous under point perturbations, as small changes can abruptly alter the spanning tree (Trofimov et al., 2023); (2) $\mathcal{L}_{\text{topo}} = 0$ is necessary but not sufficient for topological equivalence, failing to capture higher-order features like loops.

3.2. RTD-AE: Representation Topology Divergence Autoencoders

RTD-AE (Trofimov et al., 2023) addresses these limitations with stronger guarantees: nullity of RTD ensures persistence barcodes coincide across *all* homology degrees. Crucially, the loss is continuous and accounts for feature localization. The method constructs a joint distance matrix over $2n$ points:

$$D_{\text{joint}} = \begin{pmatrix} \mathbf{0}_{n \times n} & D_X^T \\ D_X & \min(D_X, D_Z) \end{pmatrix} \quad (4)$$

with loss $\mathcal{L}_{\text{RTD}} = \sum_{(b,d) \in \text{Dgm}(D_{\text{joint}})} |d - b|^p$ summing persistence lifetimes. Notably, their experiments show the gap between PCA and topological methods narrows at higher latent dimensions (64–128D). However, RTD incurs high computational cost with batch size, often requiring two-stage training (reconstruction, then topology).

3.3. Structure Preserving Autoencoders

The Structure-Preserving Autoencoder (SPAЕ) (Singh & Nag, 2021) learns low-dimensional representations where pairwise distances are a linearly scaled version of the input space distances. The method defines a distance ratio $r_{ij} = d_Z(z_i, z_j) / d_X(x_i, x_j)$ and regularizes by minimizing the variance of log-ratios:

$$\mathcal{L}_{\text{SPAЕ}} = \mathcal{L}_{\text{recon}} + \lambda \cdot \text{Var}[\log r_{ij}]_{i < j} \quad (5)$$

By operating on logarithms, the loss is scale-invariant: it permits any uniform scaling $d_Z \approx c \cdot d_X$ while penalizing non-uniform distortions. However, it relies on raw input distances, which become unreliable in high dimensions due to the curse of dimensionality. And the ratio formulation amplifies noise for small distances: when $d_X \approx \epsilon$, the ratio d_Z/d_X becomes unstable, and $\log(d_Z/d_X)$ exhibits high variance. The variant of the SPAE-graph replaces Euclidean distances with geodesic distances computed by shortest paths on a similarity graph, but introduces sensitivity to graph sparsity: holes in the data cause path detours that exaggerate distances and produce spurious geometric distortions (Lim et al., 2024).

3.4. Geometric Autoencoders

GeomAE (Nazari et al., 2023) shifts the focus from global geometry to the local geometry of the decoder $g : \mathbb{R}^n \rightarrow \mathbb{R}^d$ to prevent spurious stretching in visualizations. For a given latent point z , the pullback metric $G(z) = J_g(z)^\top J_g(z)$ captures local volume distortion and anisotropy. This distortion is visualized through indicatrices—unit spheres in the pullback metric that reveal which directions are squeezed or expanded by the decoder. GeomAE minimizes the variance of the generalized Jacobian determinant:

$$\mathcal{L}_{\text{geom}} = \text{Var}_z [\log \det(G(z))] \quad (6)$$

which encourages area-preservation and uniform scaling across the embedding.

3.5. Graph Geometry-Preserving Autoencoders

GGAE (Lim et al., 2024) replaces Euclidean distances with similarity graphs. By defining a graph with weights $K_{ij} = \exp(-\|x_i - x_j\|^2/h)$, it can be shown (Shi & Sun, 2016) that if the distribution is supported on a smooth manifold then, as the number of sampled points goes to infinity, the graph Laplacian of this weighted graph converges to the Laplace-Beltrami operator of the distribution manifold. The Riemannian distortion loss:

$$\mathcal{L}_{\text{ggae}} = \mathbb{E} [\text{Tr}(H^2) - 2\text{Tr}(H) + n], \quad H = JL^{-1}J^\top \quad (7)$$

penalizes deviation from isometry. Their Batch-Kernel method selects submatrices from a precomputed global kernel, giving mini-batches access to global structure. However, the optimal choice of bandwidth h remains highly dataset-dependent—the authors acknowledge extending to new datasets is burdensome. In cases for large datasets, the GPU makes the computation of the bandwidth efficient but at a high memory cost.

4. Manifold Matching Autoencoder

4.1. Overview

MMAE consists of an encoder $f_\theta : \mathbb{R}^D \rightarrow \mathbb{R}^d$ and decoder $g_\phi : \mathbb{R}^d \rightarrow \mathbb{R}^D$, trained with a combined reconstruction loss and distance-preservation regularization.

4.2. Reference Space

Given training data $X \in \mathbb{R}^{n \times D}$, the reference space E defines the target distance structure that the latent space should preserve. In its simplest form, $E = X$ uses the original input space directly, similarly to Singh & Nag (2021). More generally, E can be any embedding of the data:

$$E = u(X) \in \mathbb{R}^{n \times k} \quad (8)$$

where $u : \mathbb{R}^{n \times D} \rightarrow \mathbb{R}^{n \times k}$ is an embedding. This formulation provides flexibility: the embedding u can be chosen to emphasize different geometric properties—linear projections preserve global structure, while neighborhood-based methods like UMAP preserve local topology.

For high-dimensional data where distances concentrate due to the curse of dimensionality (Aggarwal et al., 2001), using a reduced embedding $E = u(X)$ with $k < D$ can provide more informative distance comparisons than the original space. The key insight is that u acts as a preprocessing step that filters noise and extracts the relevant geometric structure, which the autoencoder then learns to match. We focus on PCA as our main reference space besides the original input.

4.3. Manifold-Matching Regularization (MM-reg)

For a batch of n points with latent representations $Z \in \mathbb{R}^{n \times d}$ and reference representations $E \in \mathbb{R}^{n \times k}$ (where $k = D$ if using original input), we compute pairwise Euclidean distance matrices:

$$D_Z^{ij} = \|z_i - z_j\|_2 \quad (9)$$

$$D_E^{ij} = \|e_i - e_j\|_2 \quad (10)$$

The manifold-matching regularization is the mean squared error between these distance matrices:

$$\mathcal{R}_{\text{MM}} = \frac{1}{n^2} \sum_{i,j} (D_Z^{ij} - D_E^{ij})^2 \quad (11)$$

This directly penalizes discrepancies between latent and reference pairwise distances, encouraging the encoder to preserve the metric structure of the reference space.

4.4. Total Objective

The full MMAE objective combines reconstruction and manifold-matching:

$$\mathcal{L}_{\text{MMAE}} = \mathcal{L}_{\text{recon}} + \lambda \cdot \mathcal{R}_{\text{MM}} \quad (12)$$

Manifold-Matching Autoencoders

Dataset	Method	DC \uparrow	TA \uparrow	KL $_{0.1}\downarrow$	
Nested Spheres (101D)	Vanilla AE	-0.40	0.42	0.85	
	MMAE (Ours)	0.67	0.70	0.23	
	TopoAE	0.63	0.69	0.29	
	RTD-AE	0.61	0.69	0.29	
	GeomAE	-0.18	0.48	0.66	
	GGAE	0.11	0.54	0.46	
	SPAe	0.55	0.66	0.32	
Linked Tori (100D)	Vanilla AE	0.71	0.77	0.03	
	MMAE (Ours)	0.91	0.87	0.003	
	TopoAE	0.84	0.82	0.008	
	RTD-AE	0.90	0.86	0.005	
	GeomAE	0.77	0.78	0.01	
	GGAE	0.80	0.81	0.02	
	SPAe	0.89	0.85	0.003	
Concentric Spheres (1000D)	Vanilla AE	0.51	0.66	0.37	
	MMAE (Ours)	0.61	0.68	0.30	
	TopoAE	0.59	0.67	0.31	
	RTD-AE	0.61	0.68	0.31	
	GeomAE	0.41	0.61	0.38	
	GGAE	0.39	0.56	0.39	
	SPAe	0.59	0.67	0.32	
Mammoth (3D)	Vanilla AE	0.94	0.91	0.007	
	MMAE (Ours)	0.99	0.96	0.001	
	TopoAE	0.96	0.91	0.003	
	RTD-AE	0.97	0.92	0.002	
	GeomAE	0.95	0.91	0.007	
	GGAE	0.95	0.91	0.004	
	SPAe	0.98	0.93	0.002	
Earth (3D)	Vanilla AE	0.94	0.92	0.01	
	MMAE (Ours)	0.98	0.95	0.002	
	TopoAE	0.95	0.95	0.01	
	RTD-AE	0.87	0.90	0.02	
	GeomAE	0.94	0.92	0.009	
	GGAE	0.87	0.87	0.03	
	SPAe	0.98	0.93	0.002	

Figure 2. **2D latent spaces of synthetic shapes** Left: Quantitative metrics. Average over 5 runs (optimized for metric $KL_{0.1}$) Right: 2D Latent representations: **a)** Standard AE (Vanilla); **b)** MMAE; **c)** TopoAE; **d)** RTD-AE; **e)** GeomAE; **f)** GGAE; **g)** SPAE.

where $\mathcal{L}_{\text{recon}} = \frac{1}{n} \sum_i \|x_i - g_\phi(f_\theta(x_i))\|^2$ and λ controls the trade-off between reconstruction fidelity and structure preservation.

5. Experiments

5.1. Datasets

Synthetic Datasets: **Spheres** (Moor et al., 2020b): 10 small spheres embedded within a larger sphere in 101 dimensions, yielding 11 connected components—a standard benchmark for topology preservation. **Linked Tori:** Two interlocking tori as a Hopf Link embedded in 100 dimensions via random orthogonal projection. It does not matter the angle-of-view in a 2D representation, there is always going to be one torus overlapping the other. **Concentric Spheres:** 1000D Nested spherical shells in high dimensions with a coinciding center. **Mammoth:** 3D point cloud forming a

mammoth skeleton structure (MNoichl, 2025). **Earth:** 3D point cloud of the planet Earth globe (Nazari et al., 2023) colored by six continents: North/Central America, South America, Europe, Asia, and Oceania.

Real-World Datasets. **MNIST** and **Fashion-MNIST** (Lecun et al., 1998; Xiao et al., 2017): 28×28 grayscale images (784 dimensions). **CIFAR-10** (Krizhevsky, 2009): $32 \times 32 \times 3$ color images (3072 dimensions). **PBMC3k:** Single-cell RNA-seq data with 2,700 cells across 1,838 genes (10x Genomics, 2016), and **Paul15:** 2,730 mouse bone marrow cells across 3,451 genes (Paul et al., 2015), both representing biological manifold structure and available through the Scanpy library (Wolf et al., 2018).

5.2. Baselines

We compare against both topological and geometric autoencoder methods: **Vanilla AE**: Standard autoencoder with MSE reconstruction loss only. **TopoAE** (Moor et al., 2020b): Topological regularization via persistent homology on minimum spanning trees. **RTD-AE** (Trofimov et al., 2023): Representation Topology Divergence with joint filtration construction. **GeomAE** (Nazari et al., 2023): Geometric regularization minimizing decoder Jacobian variance. **GGAE** (Lim et al., 2024): Graph geometry preservation via Laplacian-based distortion. **SPAE** (Singh & Nag, 2021): Structure-preserving regularization via variance of log distance ratios between latent and input spaces.

5.3. Evaluation Metrics

We evaluate methods using: **Distance Correlation (DC)** and **Triplet Accuracy (TA)** which measure the preservation of the global geometry; **KL Density** (Moor et al., 2020b) at scale $\sigma = 0.1$ measuring the preservation of the density (following Moor et al. (2020b) and Trofimov et al. (2023) this is our metric to optimize hyperparameter, as this scale offers good balance of local/global density); **Wasserstein Distance** (W_0) on persistence diagrams for topological preservation of connected components; **Trustworthiness (Trust)** and **Continuity (Cont)** (Venna & Kaski, 2001) which are complementary metrics for the preservation of the local neighborhood at scales $k \in \{5, 10, 50, 100\}$; and **Reconstruction Error (Rec)** as MSE.

5.4. Implementation Details

All methods use MLP architectures following Moor et al. (2020b): encoder with symmetric decoder, ReLU activations, weight decay, Adam optimizer (Kingma & Ba, 2017), and batch normalization. A CNN is used for CIFAR10. Hyperparameters such as learning rate, batch size as well as specifics of each model are chosen following a similar optimization procedure of Moor et al. (2020b); Trofimov et al. (2023). Batch sizes were chosen within a range [16; 256] (with the exception of RTD which has a batch size limited to at most 80 due to its significant increase in training time for larger batches), learning rate [10^{-4} ; 10^{-2}]. In the case of MMAEs, for real-world datasets, we allow the hyperparameter choice to use a lower dimensional PCA projection down to 80% of the original data dimensionality using Scikit (Pedregosa et al., 2011) PCA implementation, to fight the noise in the distances and help with the curse of dimensionality (Aggarwal et al., 2001). The number of trials in the optimization step is 20 for each model, and the metric to optimize is the KL Density ($\sigma = 0.1$), same as (Moor et al., 2020b; Trofimov et al., 2023) which measures the preservation of density across the whole representation, a metric tightly bound to the topological variants objectives. The

models with the best configurations are retrained 5 times, and the average on the test sets is reported.

5.5. Results

Synthetic Datasets: In the **nested spheres** (Figure 2), models inverting outer and inner spheres achieved negative DC. Only MMAE and topological variants recover the nesting relationship; GGAE shows inconsistent nesting (DC of 0.11). MMAE uniquely preserves the gap between spheres, while TopoAE and RTD-AE produce continuous embeddings. In **linked tori**, other methods produce a "bowtie" effect by compressing the overlap region, whereas MMAE maintains constant circular shapes. Despite both tori overlapping in a large region, MMAE achieves the highest DC, TA and lowest $KL_{0.1}$, finding a nonlinear point arrangement that optimizes density preservation. The **concentric spheres** by MMAE shows five distinct disks with visible gaps; TopoAE, RTD-AE, and SPAE produce continuous embeddings with no gaps. On the **mammoth**, RTD-AE, TopoAE, GeomAE, and SPAE spread the rib cage and hips to preserve local structure. Interestingly, our projection seems to improve on the MDS projection by choosing a side view of the mammoth similarly to other models but preserving the global proportions making a more realistic projection of the animal. Even though MMAE collapses one side of the rib cage onto the other instead of spreading, it still achieves the highest DC, TA and lowest $KL_{0.1}$, balancing local and global structure. The **Earth** dataset complements nested spheres results: MMAE creates distortions in South America to better preserve relative distance to Africa, and on Oceania to approximate it to Asia achieving best performance. Other methods stretch different continents in different directions significantly increasing oceanic distances (for example from Madagascar to New Zealand); RTD-AE projects South America's tip nearly into Europe. SPAE's regularization produces even stretching also performing well. GGAE showed high sensitivity to bandwidth choice on both 3D dataset, often producing circular representations ignoring data topology.

Real-world Datasets: Both MMAE and SPAE achieve W_0 competitive with RTD-AE and TopoAE, improving with bottleneck dimensionality (visible in **CIFAR10** at 128D). These distance-based methods also show superior Trust. and Cont. against GeomAE and GGAE. On **Paul15** and **PBMC3K**, MMAE achieves the lowest W_0 with highest DC and TA. These high-dimensional, relatively small datasets benefit from PCA-based MM-reg which reduces reference dimensionality to ignore noise; SPAE using raw distances performs significantly lower on Paul15 (2D bottleneck), though this weakness vanishes at larger bottlenecks. SPAE's more relaxed distance preservation provides flexibility for better connectivity (W_0) at the cost of global geometry (Ta-

Table 1. Representation quality on real-world datasets. Best per dataset in **bold**. Latent space dimensionality for each dataset: *Paul15* (2D), *MNIST* (16D), *FMNIST* (64D), *PBMC3K* (64D), *CIFAR10* (128D).

Dataset	Method	Rec↓	DC↑	TA↑	KL _{0.1} ↓	Trust↑	Cont↑	W ₀ ↓
Paul15	Vanilla AE	0.94	0.42	0.58	0.14	0.67	0.70	272.1
	MMAE (Ours)	0.94	0.85	0.77	0.07	0.69	0.82	269.5
	TopoAE	0.95	0.50	0.67	0.07	0.67	0.80	269.5
	RTD-AE	0.96	0.58	0.69	0.07	0.66	0.79	269.9
	GeomAE	0.94	0.37	0.59	0.12	0.68	0.71	273.2
	GGAE	0.94	0.23	0.57	0.13	0.63	0.65	277.2
	SPAE	0.96	0.59	0.68	0.08	0.65	0.76	269.5
MNIST	Vanilla AE	0.15	0.95	0.82	0.002	0.93	0.95	85.65
	MMAE (Ours)	0.15	0.99	0.89	0.001	0.96	0.98	71.01
	TopoAE	0.17	0.90	0.85	0.005	0.96	0.97	68.19
	RTD-AE	0.14	0.97	0.87	0.001	0.97	0.98	56.69
	GeomAE	0.15	0.79	0.78	0.01	0.93	0.93	90.10
	GGAE	0.56	0.80	0.70	0.01	0.87	0.92	43.02
	SPAE	0.39	0.97	0.87	0.001	0.96	0.97	53.87
FMNIST	Vanilla AE	0.12	0.92	0.86	0.005	0.98	0.98	26.46
	MMAE (Ours)	0.11	0.99	0.95	0.001	1.00	1.00	26.47
	TopoAE	0.12	0.94	0.86	0.004	0.98	0.98	31.81
	RTD-AE	0.09	0.99	0.95	0.001	1.00	1.00	8.08
	GeomAE	0.12	0.91	0.86	0.007	0.98	0.98	31.40
	GGAE	0.20	0.71	0.77	0.02	0.94	0.94	70.23
	SPAE	0.14	0.98	0.94	0.004	0.99	0.99	21.58
PBMC3k	Vanilla AE	0.87	0.67	0.68	0.03	0.70	0.75	238.8
	MMAE (Ours)	0.82	0.80	0.73	0.02	0.82	0.86	63.42
	TopoAE	0.82	0.72	0.74	0.02	0.82	0.87	114.5
	RTD-AE	0.88	0.70	0.70	0.03	0.77	0.82	108.7
	GeomAE	0.82	0.63	0.69	0.03	0.71	0.78	213.5
	GGAE	0.87	0.15	0.54	0.17	0.62	0.53	175.2
	SPAE	0.86	0.68	0.69	0.03	0.75	0.79	75.38
CIFAR10	Vanilla AE	0.27	0.93	0.89	0.01	0.98	0.98	21.73
	MMAE (Ours)	0.10	1.00	0.98	0.000	1.00	1.00	1.87
	TopoAE	0.14	1.00	0.97	0.001	1.00	1.00	2.95
	RTD-AE	0.16	0.99	0.95	0.005	1.00	1.00	5.80
	GeomAE	0.95	0.43	0.68	0.10	0.84	0.81	171.2
	GGAE	0.20	0.71	0.75	0.05	0.90	0.89	79.41
	SPAE	0.09	1.00	0.98	0.000	1.00	1.00	1.57

ble 1). Both regularizations enforcing global geometry produce topology preservation effects.

6. Discussion and Conclusion

6.1. Scalability

Figure 3 shows training time scaling with batch size. RTD-AE is limited to batch sizes of 80 before becoming prohibitive; TopoAE also scales poorly. Since batch topology approximates global topology only as batch size increases (Moor et al., 2020b;a), these methods face a fundamental tension. MMAE scales similarly to vanilla autoencoders and geometric variants. MMAE also achieves similar geometric fidelity to classical MDS while requiring significantly less memory through batch-wise optimization.

6.2. Two Philosophies for Impossible Embeddings

Topological methods like TopoAE and RTD-AE optimize for topological signatures—birth and death of features across scales—ensuring the latent space mirrors input connectivity. They allow distortions in order to maintain connections in the data. The linked tori is an example of this effect, in which the “bowtie” shape appears because the areas overlapping are minimized (here all models show this effect except for MMAE). Although this may be useful for downstream tasks (Hofer et al., 2017), it loses visual interpretation.

Geometric methods like GeomAE and GGAE control the stretching of the representation. In the mammoth case this means that GeomAE flattens the skeleton producing an equally stretched representation which loses proportions. In the Earth dataset, this means all continents will be

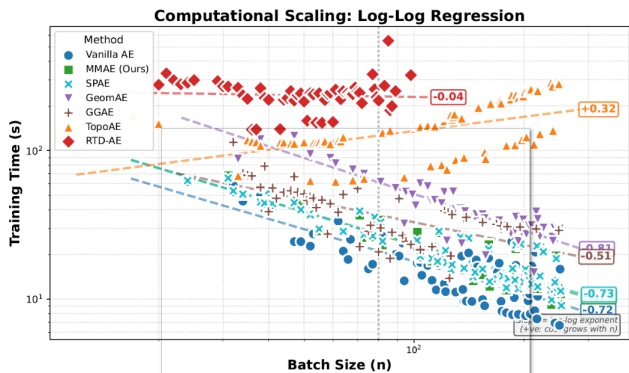


Figure 3. Training time versus batch size. MMAE scales similarly to the standard AE (Vanilla). RTD-AE limited to batch size of 80.

stretched equally which can give different visual results for each continent. This method then loses the global structure of the data in order to equally stretch. GGAE, however seems to preserve some global structure but is more difficult to finetune for each dataset, recognized by the authors Lim et al. (2024), producing a nested relationship in the nested spheres case but losing all structural information for the two 3D datasets (mammoth and Earth), which limits our interpretation of the results. MMAE and SPAE, instead, preserve global geometric relationships, which, given our results, has shown topology-preserving properties. In comparison to SPAE (Singh & Nag, 2021), which measures variance ratios in distances, MMAE better preserves global geometry proportions. On noisy high-dimensional datasets like PBMC3K and Paul15, SPAE shows lower DC, TA, Trust., and Cont. We hypothesize MMAE succeeds here because it can use reduced PCA dimensionality (down to 80%) to mitigate noise effects.

In summary, our quantitative as well as qualitative results seem to confirm the theory that topology preserving properties can be achieved by alignment of the pairwise distance matrices at the batch level. We hypothesize that one way to optimize the topology preservation would be to vary the regularization strength, by starting with a strong MM-reg regularization (high λ and then a relaxation of the parameter allowing the model to better reconstruct once it reaches a favorable representation. For example in the nested spheres case, once the model achieves the nesting relationship, even if $\lambda \rightarrow 0$, the nesting structure is maintained.

6.3. Parameterizing External Representations

Since MM-reg only requires pairwise distances, it can encode arbitrary reference representations. Duque et al. (2023) forced autoencoders to match reference coordinates directly, but Figure 1 shows MM-reg achieves similar effects: 2D representations from UMAP, t-SNE, and PCA can be copied into the latent space. This is more generic—Duque et al.

(2023) could not reproduce results in Figure 2 without an external embedding mechanism.

6.4. Limitations and Future Directions

MMAE preserves global geometry rather than explicitly preserving topology. It does not unfold manifolds but minimizes pairwise distance discrepancies, so results vary by dataset. A middle ground may exist: applying MM-reg to random point subsets could relax geometric constraints, balancing topology and geometry without persistent homology. Another interesting approach would be to combine the methods shown above to optimize the training time while getting the best of both worlds. For example, starting with MM-reg which doesn't offer significant computational overhead to capture global geometry and then concluding with the regularization of TopoAE or RTD-AE during the final epochs to enhance connectivity.

Given continued use of MDS in clustering (Chen et al., 2025) and PCA-like autoencoders (Casella et al., 2022; Ladjal et al., 2019; Pham et al., 2022), plus evidence that latent geometry (Chadebec & Allasonnière, 2022) and density (Xu et al., 2024) improve generative quality, extending MMAE to generative scenarios is promising—particularly beyond 2D/3D bottlenecks where interpolation and sampling tasks may benefit from topology preservation.

6.5. Conclusion

We presented Manifold-Matching Autoencoders, a framework for global geometry preservation through pairwise distance alignment leading to topology-preserving effect without significant computational overhead. Unlike MDS, it enables out-of-sample extension and scales to large datasets. Using PCA references allows approximating true global geometry while ignoring noise inherent to high-dimensional data. The approach also enables copying representations from other dimensionality reduction algorithms, providing out-of-sample extension for nonparametric methods. In scenarios beyond visualization, this naive distance alignment proves to be increasingly more competitive in terms of topology preservation, paving the way for the study of topology awareness in scenarios requiring larger bottlenecks.

Impact Statement

This paper presents work whose goal is to advance the field of Machine Learning. There are many potential societal consequences of our work, none which we feel must be specifically highlighted here.

References

10x Genomics. 3k PBMCs from a Healthy Donor. Single

- Cell Gene Expression Dataset, Version 1.1.0, 2016. URL <https://www.10xgenomics.com/datasets/3-k-pbm-cs-from-a-healthy-donor-1-standard>. Accessed via Scanpy datasets.
- Aggarwal, C. C., Hinneburg, A., and Keim, D. A. On the surprising behavior of distance metrics in high dimensional spaces. In *Proceedings of the 8th International Conference on Database Theory, ICDT '01*, pp. 420–434, Berlin, Heidelberg, 2001. Springer-Verlag. ISBN 3540414568.
- Batson, J., Haaf, C. G., Kahn, Y., and Roberts, D. A. Topological obstructions to autoencoding. *Journal of High Energy Physics*, 2021(4), 2021. ISSN 1029-8479. doi: 10.1007/jhep04(2021)280. URL [http://dx.doi.org/10.1007/JHEP04\(2021\)280](http://dx.doi.org/10.1007/JHEP04(2021)280).
- Borg, I. and Groenen, P. J. F. *Modern Multidimensional Scaling Theory and Applications*. Springer, New York, 2005. ISBN 038728981X. doi: 10.1007/0-387-28981-X.
- Carlsson, G. Topology and data. *Bulletin of the American Mathematical Society*, 46(2):255–308, 2009.
- Casella, M., Dolce, P., Ponticorvo, M., and Marocco, D. From principal component analysis to autoencoders: a comparison on simulated data from psychometric models. In *2022 IEEE International Conference on Metrology for Extended Reality, Artificial Intelligence and Neural Engineering (MetroXRINE)*, pp. 377–381, 2022. doi: 10.1109/MetroXRINE54828.2022.9967686.
- Chadebec, C. and Allasonnière, S. A geometric perspective on variational autoencoders. *Advances in Neural Information Processing Systems*, 35:19618–19630, 2022.
- Chari, T. and Pachter, L. The specious art of single-cell genomics. *PLOS Computational Biology*, 19(8):1–20, 08 2023. doi: 10.1371/journal.pcbi.1011288. URL <https://doi.org/10.1371/journal.pcbi.1011288>.
- Chazal, F., De Silva, V., Glisse, M., and Oudot, S. *The structure and stability of persistence modules*. Springer, 2016.
- Chen, G., Wang, X., Sun, Q., and Tang, Z.-Z. Multidimensional scaling improves distance-based clustering for microbiome data. *Bioinformatics*, 41(2):btaf042, 01 2025. ISSN 1367-4811. doi: 10.1093/bioinformatics/btaf042. URL <https://doi.org/10.1093/bioinformatics/btaf042>.
- Chen, S. and Guo, W. Auto-encoders in deep learning—a review with new perspectives. *Mathematics*, 11(8):1777, 2023. doi: 10.3390/math11081777. URL <https://doi.org/10.3390/math11081777>.
- Cohen-Steiner, D., Edelsbrunner, H., and Harer, J. Stability of persistence diagrams. *Discrete & Computational Geometry*, 37(1):103–120, 2007.
- Duque, A. F., Morin, S., Wolf, G., and Moon, K. R. Geometry regularized autoencoders. *IEEE Transactions on Pattern Analysis and Machine Intelligence*, 45(6):7381–7394, 2023. doi: 10.1109/TPAMI.2022.3222104.
- Edelsbrunner, Letscher, and Zomorodian. Topological persistence and simplification. *Discrete & computational geometry*, 28(4):511–533, 2002.
- Hinton, G. E. and Salakhutdinov, R. R. Reducing the dimensionality of data with neural networks. *Science*, 313(5786):504–507, 2006. doi: 10.1126/science.1127647. URL <https://www.science.org/doi/abs/10.1126/science.1127647>.
- Hofer, C., Kwitt, R., Niethammer, M., and Uhl, A. Deep learning with topological signatures. In *Proceedings of the 31st International Conference on Neural Information Processing Systems, NIPS'17*, pp. 1633–1643, Red Hook, NY, USA, 2017. Curran Associates Inc. ISBN 9781510860964.
- Kingma, D. P. and Ba, J. Adam: A method for stochastic optimization, 2017. URL <https://arxiv.org/abs/1412.6980>.
- Krizhevsky, A. Learning multiple layers of features from tiny images. Technical report, University of Toronto, 2009.
- Ladjal, S., Newson, A., and Pham, C.-H. A pca-like autoencoder, 2019. URL <https://arxiv.org/abs/1904.01277>.
- Lecun, Y., Bottou, L., Bengio, Y., and Haffner, P. Gradient-based learning applied to document recognition. *Proceedings of the IEEE*, 86(11):2278–2324, 1998. doi: 10.1109/5.726791.
- Lim, J., Kim, J., Lee, Y., Jang, C., and Park, F. C. Graph geometry-preserving autoencoders. In Salakhutdinov, R., Kolter, Z., Heller, K., Weller, A., Oliver, N., Scarlett, J., and Berkenkamp, F. (eds.), *Proceedings of the 41st International Conference on Machine Learning*, volume 235 of *Proceedings of Machine Learning Research*, pp. 29795–29815. PMLR, 21–27 Jul 2024. URL <https://proceedings.mlr.press/v235/lim24a.html>.
- McInnes, L., Healy, J., Saul, N., and Großberger, L. Umap: Uniform manifold approximation and projection. *Journal of Open Source Software*, 3(29):861, 2018. doi: 10.21105/joss.00861. URL <https://doi.org/10.21105/joss.00861>.

- MNoichl. Mnoichl/umap-examples-mammoth: 0.0.1, October 2025. URL <https://doi.org/10.5281/zenodo.17290165>.
- Moon, K. R., van Dijk, D., Wang, Z., Chen, W., Hirn, M. J., Coifman, R. R., Ivanova, N. B., Wolf, G., and Krishnaswamy, S. Phate: A dimensionality reduction method for visualizing trajectory structures in high-dimensional biological data. *bioRxiv*, 2017. doi: 10.1101/120378. URL <https://www.biorxiv.org/content/early/2017/03/24/120378>.
- Moor, M., Horn, M., Borgwardt, K., and Rieck, B. Challenging euclidean topological autoencoders. In *NeurIPS 2020 Workshop on Topological Data Analysis and Beyond*, 2020a. URL <https://openreview.net/forum?id=P3dZuOUnyEY>.
- Moor, M., Horn, M., Rieck, B., and Borgwardt, K. Topological autoencoders. In *Proceedings of the 37th International Conference on Machine Learning (ICML)*, Proceedings of Machine Learning Research. PMLR, 2020b.
- Nazari, P., Damrich, S., and Hamprecht, F. A. Geometric autoencoders - what you see is what you decode. In Krause, A., Brunskill, E., Cho, K., Engelhardt, B., Sabato, S., and Scarlett, J. (eds.), *Proceedings of the 40th International Conference on Machine Learning*, volume 202 of *Proceedings of Machine Learning Research*, pp. 25834–25857. PMLR, 23–29 Jul 2023. URL <https://proceedings.mlr.press/v202/nazari23a.html>.
- Paul, F., Arkin, Y., Giladi, A., Jaitin, D. A., Kenigsberg, E., Keren-Shaul, H., Winter, D., Lara-Astiaso, D., Gury, M., Weiner, A., David, E., Cohen, N., Lauridsen, F. K. B., Haas, S., Schlitzer, A., Mildner, A., Ginhoux, F., Jung, S., Trumpp, A., Porse, B. T., Tanay, A., and Amit, I. Transcriptional heterogeneity and lineage commitment in myeloid progenitors. *Cell*, 163(7):1663–1677, Dec 2015. doi: 10.1016/j.cell.2015.11.013. PMID: 26627738.
- Pedregosa, F., Varoquaux, G., Gramfort, A., Michel, V., Thirion, B., Grisel, O., Blondel, M., Prettenhofer, P., Weiss, R., Dubourg, V., Vanderplas, J., Passos, A., Cournapeau, D., Brucher, M., Perrot, M., and Duchesnay, E. Scikit-learn: Machine learning in Python. *Journal of Machine Learning Research*, 12:2825–2830, 2011.
- Pham, C.-H., Ladjal, S., and Newson, A. PCA-AE: Principal Component Analysis Autoencoder for Organising the Latent Space of Generative Networks. *Journal of Mathematical Imaging and Vision*, 64(5):569–585, June 2022. doi: 10.1007/s10851-022-01077-z. URL <https://hal.science/hal-03713275>.
- Rosenblatt, F. *Principles of Neurodynamics: Perceptrons and the Theory of Brain Mechanisms*. Cornell Aeronautical Laboratory Report No. VG-1196-G-8. Spartan Books, 1962. Original from the University of Michigan, digitized on 27 Nov. 2007.
- Schoenberg, I. J. Remarks to maurice frechet’s article “sur la definition axiomatique d’une classe d’espace distances vectoriellement applicable sur l’espace de hilbert”. *Annals of Mathematics*, 36(3):724–732, 1935.
- Shi, Z. and Sun, J. Convergence of the laplace-beltrami operator from point cloud, 2016. URL <https://arxiv.org/abs/1403.2141>.
- Singh, A. and Nag, K. Structure-preserving deep autoencoder-based dimensionality reduction for data visualization. In *2021 IEEE/ACIS 22nd International Conference on Software Engineering, Artificial Intelligence, Networking and Parallel/Distributed Computing (SNPD)*, pp. 43–48, 2021. doi: 10.1109/SNPD51163.2021.9705000.
- Su, Z., Liu, X., Hamdan, L. B., Maroulas, V., Wu, J., Carlsson, G., and Wei, G.-W. Topological data analysis and topological deep learning beyond persistent homology: A review. 59(2):58. ISSN 1573-7462. doi: 10.1007/s10462-025-11462-w. URL <https://doi.org/10.1007/s10462-025-11462-w>.
- Torgerson, W. S. Multidimensional scaling: I. Theory and method. *Psychometrika*, 17(4):401–419, 1952.
- Trofimov, I., Cherniavskii, D., Tulchinskii, E., Balabin, N., Barannikov, S., and Burnaev, E. Learning topology-preserving data representations. In *International Conference on Learning Representations*, 2023. URL <https://openreview.net/forum?id=1Iu-ixf-Tzf>.
- van der Maaten, L. and Hinton, G. Visualizing data using t-sne. *Journal of Machine Learning Research*, 9(86):2579–2605, 2008. URL <http://jmlr.org/papers/v9/vandermaaten08a.html>.
- Venna, J. and Kaski, S. Neighborhood preservation in nonlinear projection methods: An experimental study. In *International conference on artificial neural networks*, pp. 485–491. Springer, 2001.
- Wolf, F. A., Angerer, P., and Theis, F. J. Scanpy: large-scale single-cell gene expression data analysis. *Genome Biology*, 19(1):15, 2018. doi: 10.1186/s13059-017-1382-0. URL <https://doi.org/10.1186/s13059-017-1382-0>. PMID: 29409532.
- Xiao, H., Rasul, K., and Vollgraf, R. Fashion-mnist: a novel image dataset for benchmarking machine learning algorithms, 2017. URL <https://arxiv.org/abs/1708.07747>.

Xu, J., Le, H., and Samaras, D. Assessing sample quality via the latent space of generative models. In *Computer Vision – ECCV 2024: 18th European Conference, Milan, Italy, September 29–October 4, 2024, Proceedings, Part LIX*, pp. 449–464, Berlin, Heidelberg, 2024. Springer-Verlag. ISBN 978-3-031-73201-0. doi: 10.1007/978-3-031-73202-7_26. URL https://doi.org/10.1007/978-3-031-73202-7_26.